Manufacturing Rev. **10**, 7 (2023)

https://doi.org/10.1051/mfreview/2023006

Manufacturing Review
Available online at:
https://mfr.edp-open.org

RESEARCH ARTICLE OPEN ACCESS

Development of OCMNO algorithm applied to optimize surface quality when ultra-precise machining of SKD 61 coated Ni-P materials

Le Anh Duc, Pham Minh Hieu, and Nguyen Minh Quang*

Hanoi University of Industry, Tu Liem District, Ha Noi, Vietnam

Received: 13 December 2022 / Accepted: 11 March 2023

Abstract. In this paper, a new algorithm developing to solve optimization problems with many nonlinear factors in ultra-precision machining by magnetic liquid mixture. The presented algorithm is a collective global search inspired by artificial intelligence based on the coordination of nonlinear systems occurring in machining processes. Combining multiple nonlinear systems is established to coordinate various nonlinear objects based on simple physical techniques during machining. The ultimate aim is to create a robust optimization algorithm based on the optimization collaborative of multiple nonlinear systems (OCMNO) with the same flexibility and high convergence established in optimizing surface quality and material removal rate (MRR) when polishing the SKD61-coated Ni-P material. The benchmark functions analyzing and the established optimization polishing process SKD61-coated Ni-P material to show the effectiveness of the proposed OCMNO algorithm. Polishing experiments demonstrate the optimal technological parameters based on a new algorithm and rotary magnetic polishing method to give the best-machined surface quality. From the analysis and experiment results when polishing magnetic SKD 61 coated Ni-P materials in a rotating magnetic field when using a Magnetic Compound Fluid (MCF). The technological parameters according to the OCMNO algorithm for ultra-smooth surface quality with Ra = 1.137 nm without leaving any scratches on the after-polishing surface. The study aims to provide an excellent reference value in optimizing the surface polishing of difficult-to-machine materials, such as SKD 61 coated Ni-P material, materials in the mould industry, and magnetized materials.

Keywords: OCMNO / MCF / polishing / optimization / nonlinear system

1 Introduction

With the rapid development of computer science in recent years, the research and application of artificial intelligence (AI) in optimization have attracted considerable research attention and action [1–3]. AI simulates human intelligence processes with machines, especially computer systems. These processes include learning (acquiring knowledge and rules for obtaining information), rationalizing (using rules to achieve approximate or final results), and self-correction. The topics around artificial intelligence are the components of artificial neural networks, expert systems, fuzzy logic, and genetic algorithms [4,5]. Among the candidates in optimization, Yang [6] introduced meta-heuristic algorithms for solving many challenging optimization problems. When considering the processes within optimization, we can understand how humanistic aspects are related to behaviours. That's why for this reason, AI has been the perfect solution for optimization problems. It is enough for us to understand the point where optimization is the subject of decision-making, AI and optimization. In this paper, we introduce a new meta-heuristic optimization algorithm called optimize cooperation many nonlinear systems (OCMNO). In addition to some standard testing functions, the proposed algorithm applies to the problem of optimizing technological parameters in the magnetic polishing process. The advantages of the proposed algorithm compared with those obtained by previous studies expresses through the following characteristics:

– Proposing an artificial intelligence inspired optimization algorithm: As opposed to previous heuristic algorithms that were inspired by evolutionary or natural phenomena, presented algorithm is based on an artificial intelligence concept. Considering the fact that personal movements of NLOs and their internal interactions are programed by human brain, a wide range of movements

* e-mail: nmqy1984@gmail.com

and characteristics can be obtained which are mostly rare or impossible to observe simultaneously in a specific creature or phenomenon in the nature. Therefore, high flexibility of implementation and programing is achievable.
– The new operators are different from those presented by previous algorithms: Three new operators have been presented in proposed optimization algorithm, which are different than those of presented by previous algorithms.
– The convergence quality of OCMNO depends on a control parameter and is limited to a short period, thereby minimising the familiar methods related to set control parameters.
– The position of the elite solutions used in the revision method helps maintain the diversity of solutions, and demonstrate strength and high convergence. While, some optimization algorithms omitted this methodology, or this the problem about other remaining algorithms like PSO and GA [7–9] results in a pre-mature convergence of algorithm and plighting in local optima.

The SKD 61 coated Ni-P material has in recent years become popular in many areas of manufacturing processes such as electronics, chemicals, plastics and aerospace and is particularly useful in the fabrication of parts in stamping dies and hot stamping dies. The resulting Ni-P coating has high corrosion resistance and wears resistance with excellent hardness which greatly improves the working life of the products thereby improving economic efficiency and reducing costs in production processes [10,11]. The previous surface finishing processes for SKD61-coated Ni-P materials usually used grinding, however, these processes give low surface quality, which is not suitable for the manufacturing process with the ultra-fine surface of the mould industry. In order to achieve an ultra-smooth product surface in most finishing processes, a polishing process is required to remove scratches and residual stresses above or below the surface layer. Among the existing machined surface finishing techniques, grinding or polishing by abrasive particles is commonly used, however, in machining processes, it is difficult to produce super-flat surfaces without leaving residual stress or scratched, damaged surfaces [12–14]. In order to meet the requirements of machining ultra-precise and ultra-gloss surfaces, electromechanical polishing processes can be achieved but these processes have been shown to be less effective when applied to some materials [15,16]. A method is being studied in recent years for surface finishing by elastic emission machining, but the material removal capacity of this method is not high [17,18]. To overcome the disadvantages of previous methods and to produce ultra-smooth surfaces with undamaged surfaces obtained with proven efficiency and plausibility by magnetic polishing processes [19,20]. In magnetic polishing processes, the magnetic liquid mixture under the action of a magnetic field produces a non-Newtonian liquid that exists as a hard liquid strip that serves as a flexible polishing tool [21,22]. The shape and hardness of the magnetic fluid strip can be controlled through procedures that modulate the strength of the magnetic field thereby enhancing the performance of the magnetic polishing processes. In polishing processes with magnetic liquid mixtures, performance and operability are significantly influenced by the method and manner of magnetic field application [22–24]. When subjected to a constant magnetic field during machining processes with constant geometry and magnetic force distribution, it forms a fixed, inflexible magnetic polishing tool in finishing processes. Under the influence of a constant magnetic field, the ferromagnetic particles and abrasive particles present in the magnetic compound fluid (MCF) do not evenly disperse under the influence of the magnetic field, thereby not creating the expected polishing process. To overcome this phenomenon, finishing processes under the effect of a rotating magnetic field were established. The flux density is constant in the rotating magnetic field but the distribution process is always changing over time due to the ever-changing magnetic field, thereby creating geometric shapes with much improved and more uniform distribution of abrasive particles under the influence of a rotating magnetic field.

Based on the above-mentioned characteristics, aim to create a polished model with the ultra-smooth surface of material SKD61 coated Ni-P. In this study, the authors analyzed and developed a new mathematical model in optimization for nonlinear systems generated by machining processes. The authors propose a hybrid model based on the combination of the high convergence and flexibility of the proposed OCMNO algorithm with the newly developed magnetic polishing process with the rotating magnetic field in order to find the technological parameters for the ultra-smooth surface quality of SKD 61 coated Ni-P material. The optimized model along with the proposed rotating magnetic polishing process aims to further improve the surface quality, thereby providing excellent reference values for the manufacturing processes ultra-precision as well as the mould-making industry.

2 OCMNO algorithm

The structure of the proposed algorithm is described based on the coordination of nonlinear objects in the group aim to find out the optimal parameters. The algorithm diagram is shown in Figure 1. From here shown that just like other evolutionary optimization algorithms. The first step of the algorithm must set up the initial nonlinear objects (NLO) for the group. Based on the signal obtained from the NLOs, the NLO that acquires data larger than those collected by other NLOs in the group will act as the main NLO. The main NLO will then set up optimal situations for the group. Meanwhile, the other NLOs in the group must follow the control signal of the main NLO, which are called dependent NLO. When a dependent NLO reaches a location with a better data source than that obtained by the main NLO, the dependent NLO will become the main NLO and will act as a guide to the group in the next part of the optimization task. Simultaneously, the previous main NLO will play the role of a dependent NLO. When implementing cooperation and optimization tasks, there is always an exchange of information between NLOs. Thus, the rank of the NLOs in the group is completely related to the location and capability to track important signals emitted from the target.

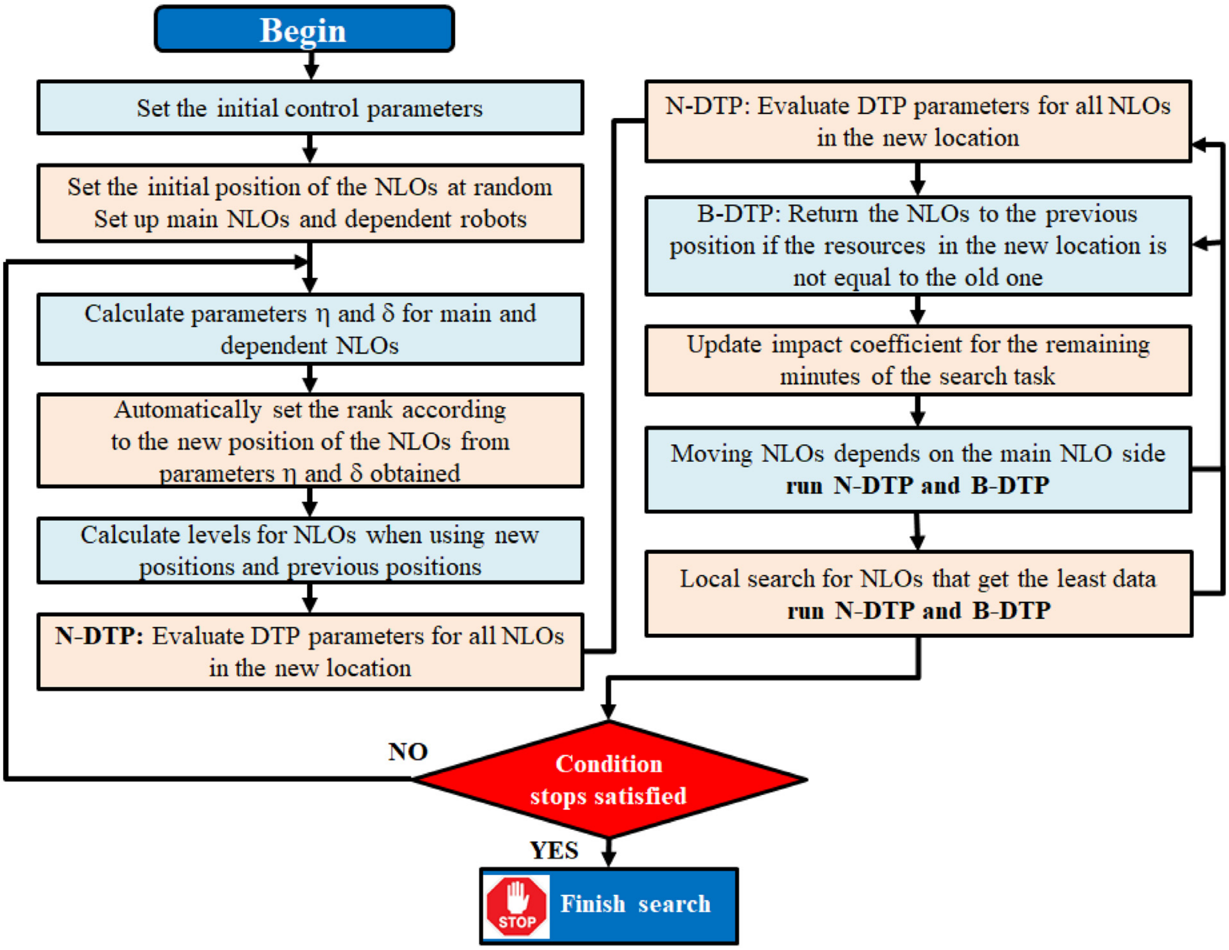

Fig. 1. Proposed OCMNO diagram.

In the mission of cooperation and optimization, with the leadership of the main NLO, the following operators are formed:

- Collection operator (concentrating NLOs depending on the position of the main NLO). The first operator moves solutions to their new positions by utilizing normal distribution function. To this end, a new method for calculating mean and variance factors for each of solutions are presented.
- Exploration operator (setting search distance between main and dependent NLOs). The second operator may displace solutions toward/backward the best solution by a twofold main-dependent concept. None of previous algorithms can lead some of solutions on counter direction of best solution during a controlled procedure to explore the entire of search space better. Besides, as opposed to previous algorithms like PSO, GA and etc. in which positions of low quality solutions were basis of their new respective positions, some positions around these solutions are basis of movement for low quality solutions in proposed operator.
- Local search operator (establishing some dependent NLOs on the task of searching around the location of the main NLO). Well-known operators of exponent and round effecting on float part of variables are employed for the first time in this paper as the third operator. These operators considerably accelerate convergence of algorithm when solutions are gathered near the most optimal position.

Compared with individuals in natural swarms, the NLOs in the group can record restrictions by previous steps. This feature allows NLOs to return to previous locations if they cannot find a convenient location during task completion.

2.1 Set up the original NLO for the group

Optimisation problems are determined by vectors of N_V decision variables to identify the position of NLOs in the search area, and the initial solution is set by an array of size $1\times N_V$. The position of the ith NLO is determined by the following equation:

$$P^i_{\mathrm{NLO}} = [x_1, x_2, \ldots, x_{N_V}], \tag{1}$$

where $i = 1, 2, \ldots, N$.

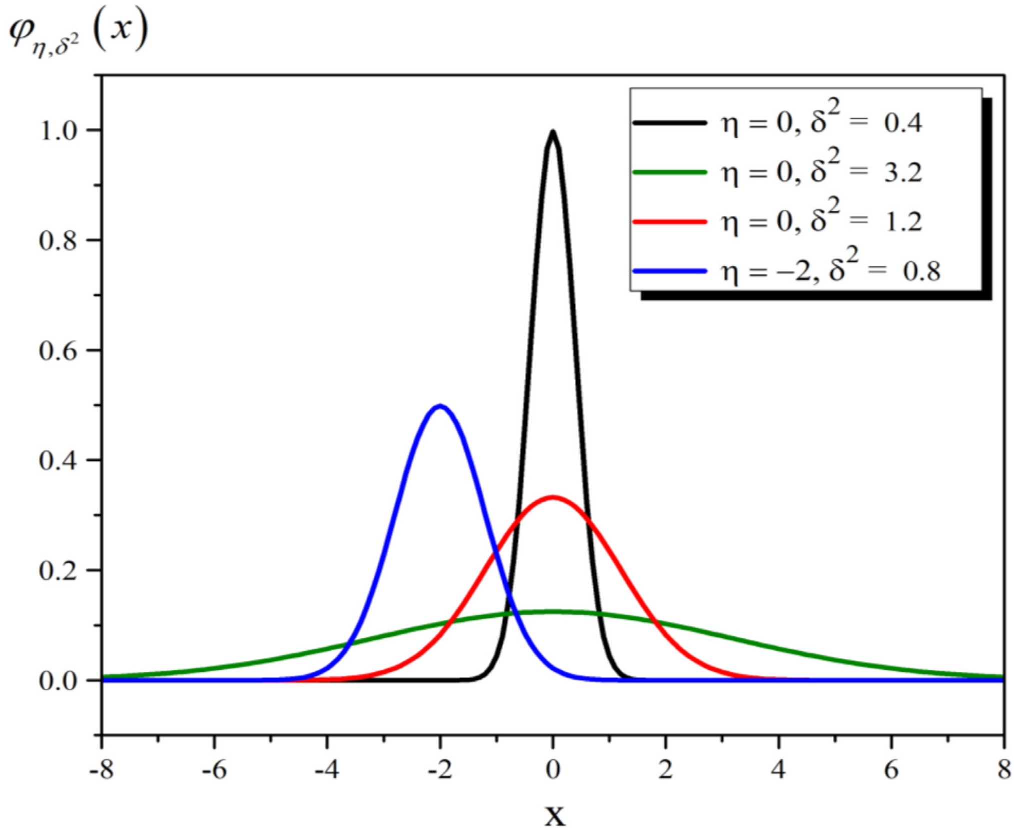

Fig. 2. Probability density function with different parameters.

The parameters of $x_1, x_2, ..., x_{N_V}$ variables are determined by location. The value that displays the optimal target parameter (DTP) is determined by the equation:

$$\text{DTP} = f(P^i_{\text{NLO}}) = f([x_1, x_2, ..., x_{N_V}]), \tag{2}$$

where $f(P^i_{\text{NLO}})$ is called optimisation function. Given that N is the number of NLOs in the group, the $N \times N_V$ matrix is created as an initial NLO population. The initial position of the NLOs is determined by the equation:

$$P_{\text{NLO}} = Ur(V_{\text{MAX}}, V_{\text{MIN}}, V_{\text{side}}), \tag{3}$$

where Ur creates a sequence of random points from a continuous uniform distribution with the lowest and highest endpoints determined by V_{MIN}, V_{MAX} and $V_{\text{size}} = 1 \times N_V$; V_{MAX} and V_{MIN} are the largest and smallest limit of decision variables, respectively.

After creating the solutions and evaluating the initial parameters, the main and dependent NLOs are determined on the basis of the DTP index.

2.2 Collection operator

After the initial setup for the main and dependent NLOs, all dependent NLOs move to the position near the main NLO position. This accumulation nearby the position of main NLO is implemented with random movements and by utilizing normal probability distribution function. The probability density of normal distribution is given by:

$$y = f[x|\eta, \delta] = \frac{1}{\delta\sqrt{2.\pi}} e^{\frac{-(x-\eta)^2}{2\delta^2}}, \tag{4}$$

where η is the average parameter, δ is the standard deviation and δ^2 is the variance. A random variable with a Gaussian distribution is said to be normally distributed and is called a normal deviate. If $\eta = 0$ and $\delta = 1$, the distribution is called the standard normal distribution denoted by N (0,1). Figure 2 shows the probability density function for normal distribution with different parameters. During cooperation and optimization tasks, parameters η and δ are used to identify the main and dependent NLOs, respectively.

2.2.1 Calculate parameters η and δ for main and dependent NLOs

When the optimization tasks, the main NLO gathers dependent NLOs to its current location to direct them on the location with the highest resource. After the dependent NLOs gather close to the position of the main NLO, the local search process is initiated. The main NLO attempts to improve its information gathering ability to implement this search method, whilst other NLOs move to the location with the highest DTP. Considering P_1 as the first control point, the parameters η and δ for the main NLO are

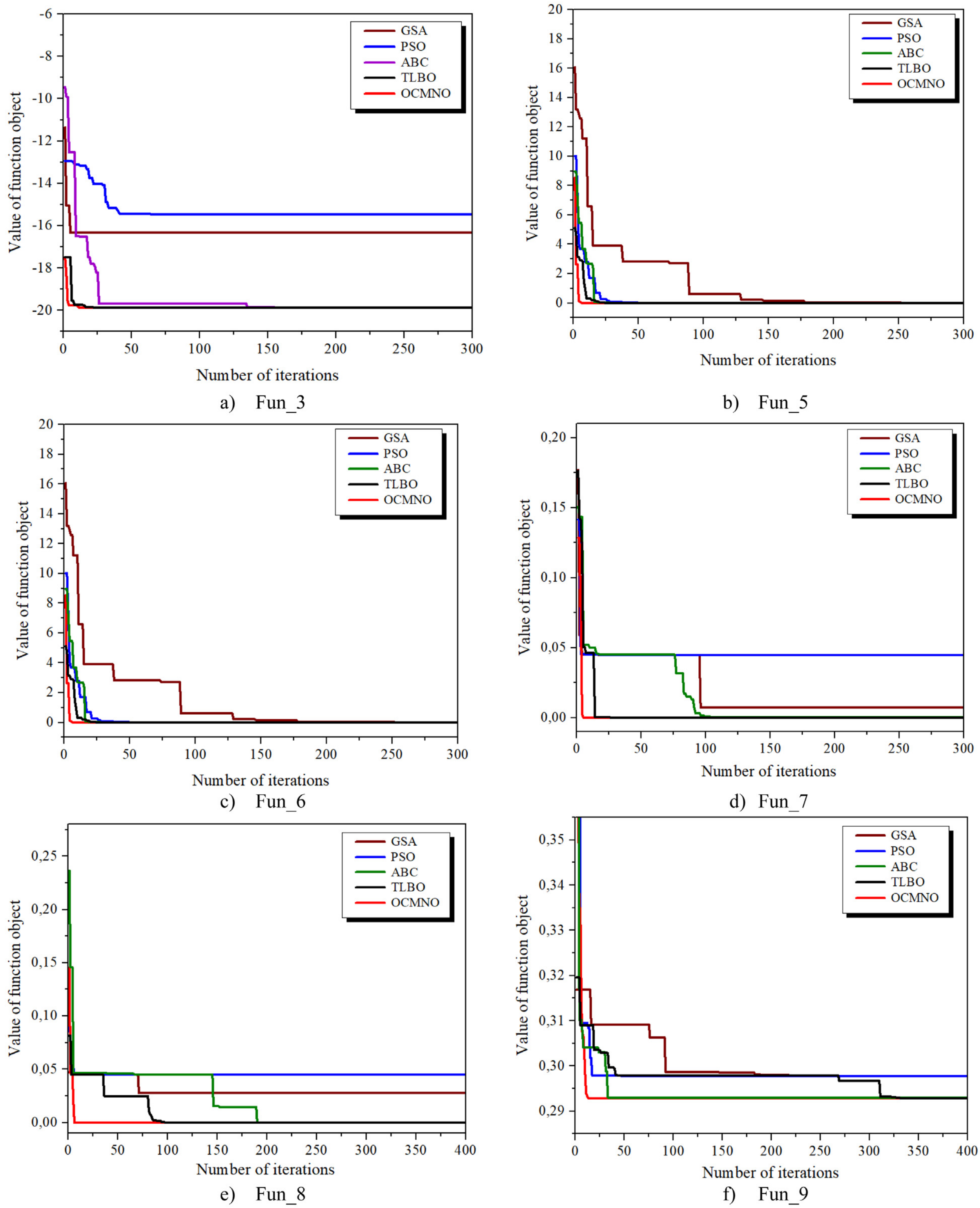

Fig. 3. Convergence capability with different optimisation algorithms.

Table 1. Calculation of DF parameters.

Step	Set up and calculate parameters	Note
1	DIF = 6	Set initial parameters (modified after repetition)
2	$\mathrm{DF}_i = \mathrm{DIF} \times k_i$	Calculation
3	$\mathrm{DTP}^i_{\text{movement}} = \mathrm{DTP}^i_{\text{NLO}} - NewDTP^i_{\text{NLO}}$	Calculation
4	Select the ith NLO	NLO has the largest DTP_{movement}
5	$\mathrm{DIF} = \left[1 + \left\{\max\left(\overline{V}_{\max} - \overline{V}_{min}\right)\right\} \times k\right] \times DTP_{\max}$	$\mathrm{DTP}_{\max}$ is selected in step 4
6	DIF is obtained in the previous step $\left[0, \max\left(\overline{V}_{\max}\right)\right]$.	The limit value comes from the principle 6δ
7	Switch back to step 2 to repeat the new round	

respectively determined by the following equation:

$$\delta_{\text{NLO}[M]} = k, \tag{5}$$

$$\eta_{\text{NLO}[M]} = \left(\frac{1 + (-1)^{E_T+1}.\delta_{\text{NLO}[M]}}{\left(\max\left[0, (-1)^{E_T+1}\right]\right).(1 - P_1) + 1}\right).P_{\text{NLO}[M]}, \tag{6}$$

where k is a random number in the range [0,1], E_T is the time taken by the search task of OCMNO and $P_{\text{NLO}[M]}$ is the location of the main NLO.

Parameters η and δ for dependent NLOs are respectively determined by the following equation:

$$\delta_{\text{NLO}[D]} = DF^i \times \left(P_{\text{NLO}[M]} - P^i_{\text{NLO}[D]}\right) + k^2 \times P^i_{\text{NLO}[M]}(j)|, \tag{7}$$

$$\eta^i_{\text{NLO}[D]} = P_1 \times P_{\text{NLO}[M]} + (1 - P_1) \times P^i_{\text{NLO}[D]}, \tag{8}$$

where $i = 1, 2, \ldots, N_D; j = 1, 2, \ldots, N_V$ and DF^i is the parameter correction factor δ for the ith dependent NLO.

2.2.2 Create new locations for main and dependent NLOs

The new position of the main and dependent NLOs is determined using parameters η and δ corresponding to each NLO

$$NewP_{\text{NLO}(i)} = Gr\left(\eta_{\text{NLO}(i)}, \delta_{\text{NLO}(i)}\right), \tag{9}$$

where the Gr function generates an array of random floating point number from NLO with parameters η and δ obtained in the previous section. The following formulas below are applied to create a relationship between the new positions obtained in the search space:

$$NewP_{\text{NLO}(i)}(j) = Max\left(V_{\text{Min}}(j), NewP_{\text{NLO}(i)}(j)\right), \tag{10}$$

$$NewP_{\text{NLO}(i)}(j) = Min\left(V_{\text{Max}}(j), NewP_{\text{NLO}(i)}(j)\right), \tag{11}$$

$$NewDTP_{\text{NLO}(i)} = f\left(NewP_{\text{NLO}(i)}\right). \tag{12}$$

2.2.3 Determine collection parameters DF

When the new position of the NLOs is set, the DF parameter will be updated and modified after every minute of the search task based on changes by DTP parameters of the NLOs in the current iteration (there is reference by the previous iteration). The calculation of DF parameters is shown in Table 1.

$\mathrm{DTP}^i_{\text{movement}}$ is determined in Step 3 before making progress assessment. Some NLOs will return to their previous position if the new locations have inappropriate $\mathrm{DTP}_{\text{NLO}}$ parameters.

2.3 Exploration operator

The exploration process is where dependent NLOs are allowed to search in their surroundings when heading to the main NLO or vice versa. The location of dependent NLOs according to this policy is determined by the following equation:

$$NewP^i_{\text{NLO}[D]} = k \times P^i_{\text{NLO}[D]} + RB \times \left(P_{\text{NLO}[M]} - P^i_{\text{NLO}[D]}\right) \times ME, \tag{13}$$

where RB = ± 1 variable is randomly selected with motion factor (ME) determined by $\max\left(1, |P_{\text{NLO}[M]} - P^i_{\text{NLO}[WD]}|\right)$ at the end of each iteration. The WD index refers to the dependent NLO with the lowest DTP. The ME parameter can control the convergence rate and the accuracy of the search process in different execution time intervals.

2.4 Local search operator

In this operator, some NLOs with the lowest quality of information obtained work as worker NLOs. These NLOs are assigned to search around the location of the main NLO. However, the residence of worker NLOs at the new location only occurs when an improved position of the second-ranked NLO is realised. Otherwise, the worker NLOs will return to their previous location after the search

Table 2. Benchmark functions.

Func.	Description	Scale B1	Scale B2	Scale B3	Range	Global minimum
Nonmodal functions						
Fun.1	$\sum_{i=1}^{N} X_i^2$	10	50	200	$[-100, 100]$	0
Fun.2	$\sum_{i=1}^{B}\left[100 \times \left(X_i^2 - x_{i+1}\right)^2 + (1 - X_i)^2\right]$	2	50	200	$[-10, 10]$	0
Fun.3	$1.1X\sin(2Y) + \sin(4X) \times Y$	2	–	–	$[-10, 10]$	–19.8625
Fun.4	$10N + \sum_{i=1}^{N}\left[X_i^2 - 10\cos(2\pi X_i)\right]$	3	50	200	$[-5.12, 5.12]$	0
Fun.5	$-20.e^{\left[-0.2\sqrt{\frac{1}{30}\sum_{i=1}^{B} X_i^2}\right]} - e^{\left[-0.2\sqrt{\frac{1}{30}\sum_{i=1}^{B}\cos(2\pi X_i)}\right]}$	10	50	200	$[-30, 30]$	$8.8818e^{-16}$
Fun.6	$\sum_{i=1}^{n}\cos(X_i).\left[X_i^2 + X_i\right]$	2	50	200	$[-10, 10]$	–100.22365*B
Fun.7	$\sum_{i=1}^{N}\left(\lvert X_i\rvert - 10.\cos\left[\sqrt{\lvert X_i\rvert}\right]\right)$	10	50	200	$[-10, 10]$	–10*B
Fun.8	$0.5 + \frac{\sin^2\left[\sqrt{\left(X_1^2+X_2^2\right)}\right]-\frac{1}{2}}{0.001\left(X_1^2+X_2^2\right)+1}$	2	–	–	$[-10, 10]$	0
Fun.9	$1 + \sum_{i=1}^{N}\frac{X_i^2}{4000} - \prod_{i=1}^{N}\cos\left[\frac{X_i}{\sqrt{i}}\right]$	10	50	200	$[-10, 10]$	0.29289

Multimodals		Range	Global minimum	Global peak
Fun.10	$X_1^2 \times \left(\frac{X_1^4}{3} + 4 - 2.1X_1^2\right) + 4 \times \left(X_2^2 - 1\right) \times X_2^2 + X_1X_2$	$x_1 \in [-1.9, 1.9]$ $x_2 \in [-1.1, 1.1]$	–1.105	2
Fun.11	$\left(X_1^2 + X_2 - 11\right)^2 + \left(X_1 + X_2^2 - 7\right)^2$	$x_1 \in [-10, 10]$ $x_2 \in [-10, 10]$	0	4
Fun.12	$\left[\sum_{i=1}^{5} i \times \cos\{(i-1)X_1 + i\}\right] \times \left[\sum_{j=1}^{5} j.\cos\{(j-1).X_2 + j\}\right]$	$x_1 \in [-10, 10]$ $x_2 \in [-10, 10]$	–176.542	18

fails. The new position of the worker NLO is determined by the following formula:

$$NewP^1_{\mathrm{NLO}[W]} = \mathrm{sign}\left[Rd^+\left(\lvert P_{\mathrm{NLO}[M]}\rvert\right)\right]_{\mathrm{NLO}[M]}, \tag{14}$$

$$NewP^2_{\mathrm{NLO}[W]} = \mathrm{sign}\left[Rd^-\left(\lvert P_{\mathrm{NLO}[M]}\rvert\right)\right]_{\mathrm{NLO}[M]}, \tag{15}$$

where Rd^+(x) and $Rd^-(x)$ are the nearest integers closest to x, and sign$[\Phi]_\Psi$ reflects the signs of element Ψ by element Φ.

$$NewP^3_{\mathrm{NLO}[W]} = \mathrm{sign}\left[RI\left(P_{\mathrm{NLO}[M]}\right) + \left\{RF\left(P_{\mathrm{NLO}[M]}\right)\right\}^{\frac{1}{e_1}}\right]_{\mathrm{NLO}[M]}, \tag{16}$$

Table 3. Small scale (B1) with non-modal functions benchmark functions.

No.	Parameter	Algorithms				
		TLBO	GSA	PSO	ABC	OCMNO
Fun.1	Best	3.25 e^{-6}	5.8265	4.15 e^{-14}	0.0369	0
	S.AD	1.81 e^{-4}	4.0362	2.69 e^{-11}	0.3498	0
Fun.2	Best	6.82 e^{-5}	0.0085	3.14 e^{-16}	5.62 e^{-7}	0
	S.AD	0.0325	0.2915	1.04 e^{-8}	0.0036	0
Fun.3	Best	−19.8625	−19.7734	−19.8625	−19.8624	−19.8625
	S.AD	5.72 e^{-04}	0.5189	1.9550	4.46 e^{-10}	1.68 e^{-06}
Fun.4	Best	0	1.0313	0	1.98 e^{-6}	0
	S.AD	8.79 e^{-13}	1.5538	1.3154	0.4332	0
Fun.5	Best	0.0028	4.8954	5.33 e^{-8}	0.1133	8.88 e^{-16}
	S.AD	0.1333	0.5293	0.4348	0.2695	0
Fun.6	Best	−200.4473	−200.4396	−200.4476	−200.4476	−200.4474
	S.AD	1.56 e^{-12}	1.3388	42.3978	2.6665	1.07 e^{-04}
Fun.7	Best	−80.2418	−45.7485	−76.7760	−76.2008	−100
	S.AD	2.8902	3.5163	4.2107	3.4835	0
Fun.8	Best	1.23 e^{-4}	3.61 e^{-5}	0	0	0
	S.AD	0.0105	0.0065	0.0218	6.66 e^{-9}	0
Fun.9	Best	6.35 e^{-5}	0.3206	0	4.38 e^{-4}	0
	S.AD	0.0165	0.1002	0.0314	0.1068	0

$$NewP^4_{\mathrm{NLO}[W]} = \mathrm{sign}\left[RI\left(P_{\mathrm{NLO}[M]}\right) + \left\{RF\left(P_{\mathrm{NLO}[M]}\right)\right\}^{e_2}\right]_{\mathrm{NLO}[M]}, \tag{17}$$

where $RI(\beta)$ and $RF(\beta)$ are return functions of the integer and the dimensionless part of the β elements, respectively; the parameters e_1 and e_2 are two random integers in the interval [2,4].

In this operator, the cross policies of the GA algorithm are applied. In particular, the new position of the fifth worker NLO is a combination of position $NewP^3_{\mathrm{NLO}[W]}$ and $NewP^4_{\mathrm{NLO}[W]}$ with random components R_1 and R_2, respectively (with $R_1 + R_2 = 100\%$).

$$NewP^5_{\mathrm{NLO}[W]} = \begin{bmatrix} \left\{R_1\%\left(NewP^3_{\mathrm{NLO}[W]}\right)\right\} \\ \left\{R_2\%\left(NewP^4_{\mathrm{NLO}[W]}\right)\right\} \end{bmatrix}. \tag{18}$$

This process is performed with certain variables to prevent sudden and chaotic changes in the locations where solutions are obtained.

2.5 Convergence and optimisation solution of OCMNO

The proposed algorithm is applied to non-modal functions (Fun.1 to Fun.9) and multimodal (Fun.10 to Fun.12) with small (B1), medium (B2) and large (B3) scales. These functions are described in Table 2.

The stop criteria of the algorithm are determined by the following formula:

$$f_{End}(Ro[M]) - Glo \leq S.CA, \tag{19}$$

where $f_{End}(Ro[M])$ is the value corresponding to the solution, which is best obtained at the last iteration of the algorithm, and S.CA is the stop criterion of the algorithm. This criterion will converge with tolerances 10^{-6} and 10^{-3} corresponding to non-modal and multimodal functions, respectively. The standard deviation with the obtained results is shown as follows:

$$S.AD = \left(\frac{1}{n}\sum_{i=1}^{n}[x_i - x]^2\right)^{\frac{1}{2}}, \tag{20}$$

where x_i is the solution result vector run by the algorithm and x is the average value of solutions determined by the following formula:

$$x = \frac{1}{n}\sum_{i=1}^{n} x_i. \tag{21}$$

The parameters in Tables 3–5 of the proposed OCMNO algorithm are compared with TLBO, GSA, PSO, and ABC after 50 times of independent implementation with the best and S.AD results obtained, which correspond to scales B1 to B3. Table 3 shows the proposed OCMNO for the best performance. The proposed OCMNO algorithm shows that the efficiency through S.AD is lower than the mentioned algorithms. Tables 4 and 5 show the superiority of

Table 4. Medium scale (B2) with non-modal functions benchmark functions.

No.	Parameter	Algorithms				
		TLBO	GSA	PSO	ABC	OCMNO
Fun.1	Best	0.0771	201.0651	85.7738	20.9615	0
	S.AD	1.1830	65.5293	95.5022	238.9055	0
Fun.2	Best	49.0557	7.15 e^4	158.6456	432.4415	48.5065
	S.AD	0.8573	4.90 e^4	152.5239	1.76 e^4	0.1061
Fun.3	Best	24.8026	478.2613	65.4385	0	0
	S.AD	42.8524	17.3122	22.4825	85.3015	0
Fun.4	Best	0.0619	8.2536	2.7345	5.9036	8.88 e^{-16}
	S.AD	0.0934	0.3456	1.0962	2.1066	0
Fun.5	Best	−4694.7	−1182.8	−2882.1	−4235.6	−4813.5
	S.AD	81.2471	134.3851	285.16	183.5909	62.75
Fun.6	Best	−299.1726	−115.5256	−350.1128	−316.7345	−500
	S.AD	11.4561	11.6326	8.5081	15.6361	0
Fun.7	Best	3.25 e^{-5}	0.9831	0.0032	0.0286	0
	S.AD	2.35 e^{-4}	0.0126	0.0216	0.1193	0
Fun.8	Best	0.0771	201.0651	85.7738	20.9615	0
	S.AD	1.1830	65.5293	95.5022	238.9055	0
Fun.9	Best	49.0557	7.15 e^4	158.6456	432.4415	48.5065
	S.AD	0.8573	4.90 e^4	152.5239	1.76 e^4	0.1061

Table 5. Large scale (B3) with non-modal functions benchmark functions.

No.	Parameter	Algorithms				
		TLBO	GSA	PSO	ABC	OCMNO
Fun.1	Best	0.6035	4.89 e^3	10114	1.36 e^5	0
	S.AD	1.4665	1.97 e^3	2378.4	2.43 e^4	0
Fun.2	Best	200.1315	4.24 e^5	41084	3.48 e^6	198.5726
	S.AD	2.8213	1.39 e^5	18630	1.55 e^6	0.0602
Fun.3	Best	18.5444	1.89 e^3	777.5746	1.47 e^3	0
	S.AD	29.4734	63.1346	65.0408	96.1149	0
Fun.4	Best	0.0858	10.2015	9.7025	18.4186	8.88 e^{-16}
	S.AD	0.0642	0.3714	0.7685	0.2469	0
Fun.5	Best	−17853	−3206.5	−7706.1	−11734	−18014
	S.AD	226.7121	273.3312	1638.1	505.3369	407.7908
Fun.6	Best	−636.7332	−489.0826	−789.6431	−957.4023	−2000
	S.AD	68.1022	51.9533	50.7421	133.2738	0
Fun.7	Best	4.05 e^{-5}	1.1069	0.5448	1.3414	0
	S.AD	1.28 e^{-4}	0.0168	0.0936	0.523	0
Fun.8	Best	0.6035	4.89 e^3	10114	1.36 e^5	0
	S.AD	1.4665	1.97 e^3	2378.4	2.43 e^4	0
Fun.9	Best	200.1315	4.24 e^5	41084	3.48 e^6	198.5726
	S.AD	2.8213	1.39 e^5	18630	1.55 e^6	0.0602

Table 6. Optimal solution with multimodal functions.

Func.	Characteristics	Optimization algorithms				
		GSA	PSO	ABC	TLBO	OCMNO
Fun.10	Time reached	33	46	48	49	8.03
	Average value	−0.9784	−1.0175	−1.02803	−1.03151	−1.03162
	OA value	1.69	1.89	1.93	1.98	2
Fun.11	Time reached	30	37	40	43	47
	Average value	4.52 15 e^{-3}	5.7579 e^{-6}	3.2535 e^{-6}	4.2859 e^{-7}	4.6293 e^{-8}
	OA value	2.67	3.49	3.55	3.63	3.79
Fun.12	Time reached	18	29	32	34	40
	Average value	−152.2436	−169.5681	−170.8427	−173.8542	−175.7125
	OA value	8.01	11.79	12.67	13.39	16.98

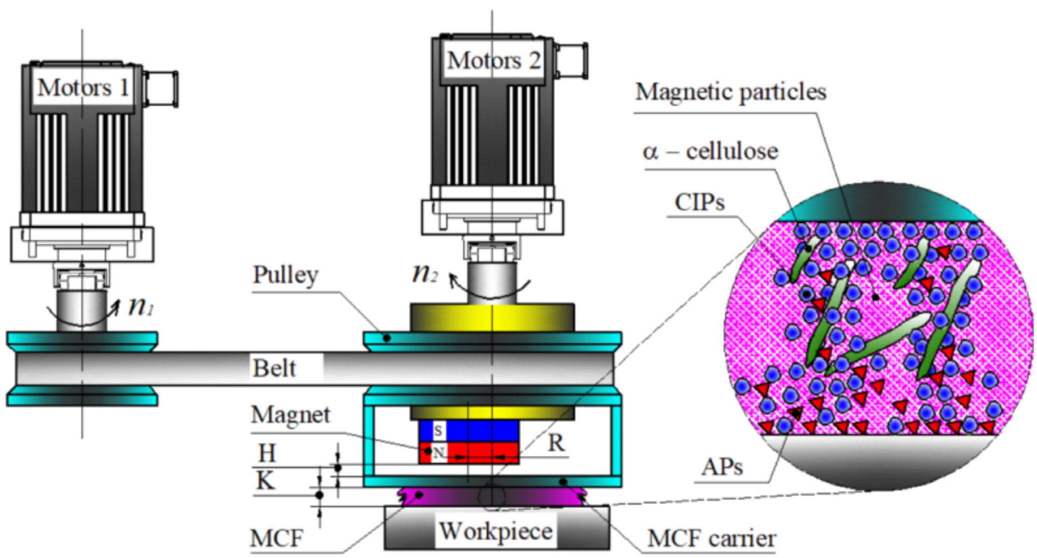

Fig. 4. Schematic diagram and experimental setup for polishing the SKD 61 coated Ni-P material in a rotating magnetic field.

OCMNO to the other algorithms by medium- and large-scale benchmark functions. Hence, with benchmark objective functions, in terms of solutions and quality, OCMNO shows superiority to other well-known algorithms.

When applying algorithms for multimodal functions (Fun.10, Fun.12) based on time, the average value (mean value of all algorithm runs) and the optimal average value (average number of peaks found above 50 times with S.CA = 1000) are shown in Table 6. Based on the results, the possibility of multimodal functions is not as high as that of non-modal functions. The complexity of the benchmark functions from Fun.10 to Fun.12 increases, thereby realising the reduction of the quality of solutions. This process is expressed via analysis. The average optimisation value (AO) corresponding to the Fun.10 function is 2 (100% success rate). However, the AO value with Fun.12 function achieved by OCMNO is 16.98 (94.3% success rate). The results show that the quality obtained by OCMNO is superior to the algorithms mentioned in most cases. Therefore, OCMNO has high applicability on target identification with nonlinear systems and various optimisation problems.

3 Applying the OCMNO algorithm in optimizing the polishing process with the MCF rotating magnetic field of SKD 61 coated Ni-P material

Figure 4 describes the polishing principle of SKD 61 coated Ni-P material using an MCF in a rotating magnetic field. The principle of creating a rotating magnetic field by a permanent magnet placed eccentrically with a distance R below the rotating disk is to create a variable magnetic field. The MCF composite is placed below the permanent magnet and a distance of H from the magnet by means of an aluminium carrier disc. Axis 2 during rotation will transmit rotational motion n_2 to the permanent magnet, under the

Table 7. MCF components set up.

Description	Parameters	Relative permeability	Material
Permanent magnets	ϕ30 × 20 mm	1.09977	Nd-FeB loại N50 $B = 0.45$T
SKD61 coated Ni-P material	ϕ20 × 10 mm		
MCF carrier disc		1	Al
Percentage of components in MCF			
CIP (Carbonyl iron particles)	2 μm	44%	Ferromagnetic
	4 μm	44%	
	6 μm	44%	
	8 μm	44%	
AP (Abrasive particles)	5 μm	8%	Al_2O_3
	3 μm	8%	
	1 μm	8%	
	0.5 μm	8%	
Deionized water		45%	
α-cenluloses		3%	

rotating action of the magnet, the magnetic force continuously rotates around axis 2, this process forms a rotating magnetic field applied to the polishing process by MCF. The MCF polishing is established when the workpiece is placed under the MCF carrier plate with a distance of K.

When a rotating magnetic field is applied, the shape and geometrical position of the assemblies will always change due to the magnetic attraction. This leads to a change in the external shape and size of the MCF composite. In the MCF polishing setup, a rotating magnetic field is generated based on a permanent magnet made of Nd50 type Nd-FeB material of cylindrical shape with a diameter of 30 mm and a thickness of 20 mm with a magnetic field strength $B = 0.45$T. The composition of the MCF is shown in Table 7.

Under the effect of the magnetic field when the MCF polishing processes are established, micrometre-sized magnetic particles are formed in the magnetic induction directions. Under the effect of magnetic particles combined with α-cellulose fibres present in the MCF during operation, the magnetic abrasive particles will follow the action of the magnetic induction line under the effect of the magnetic field. When the $n1$ motor rotates, it will transmit motion to the aluminium disc, through which the MCF polishing mixture will transmit rotation to the abrasive particles thereby creating a cutting action with a very small depth of cut by micro-sized abrasive particles.

The design of the experiment using the Taguchi orthogonal array approach can economically satisfy the needs of solving the problem and product design optimization projects. By applying Taguchi's method researchers, engineers and scientists can reduce the time, resources, and money required for little experimental investigation. Taguchi experimental design L16 is a commonly used method in investigating the impact factors, including multiple factors and levels [25,26]. This method was successfully applied to many different subjects with the aim to save time and money and obtain optimal objectives [27,28]. The key to this approach is to create an orthogonal design table on the basis of the factors and levels of impact that are being investigated. In this work, polishing parameters conducted according to Taguchi L16 experimental analysis after 60 min of polishing are described in Tables 8 and 9. The SKD 61-coated Ni-P workpieces after polishing repeated three times were averaged for material removal rate(MRR) and surface roughness at three different locations by the Zygo 7100 roughness measuring device and have an accuracy of surface topography measurement in Ra less than 0.12 nm.

The workpieces are cleaned with acetone and ethanol then dried before polishing. The workpieces were weighed before and after polishing with a high-resolution electronic balance (0.1 mg) to determine MRR. In this case, the MRR is determined by the following equation:

$$\mathrm{MRR} = \frac{\Delta m \quad 10^3}{T}, \tag{22}$$

where Δm (g) is the difference between the workpiece weight before and after polishing, T (min) is polishing time and MRR (mg/min) is material removal rate.

The results in Figure 5 show the ANOVA analysis of surface quality minimumwith experimental parameters described in Table 9 for the S/N ratio corresponds to the workpiece speed, abrasive particle diameter, ferromagnetic particle size, and magnet speed are (-12.70), (-9.38), (-13.35) and (-13.71) levels for 1313 levels (corresponding workpiece speed $n_1 = 300$ rpm; AP diameter 1 μm; AP diameter 6 μm; magnetic speed $n_2 = 60$ rpm).

Table 8. Technological parameters when polishing Ni-P SKD 61 material under rotating magnetic field.

Level	Workpiece speed n_1	AP diameter	CIP diameter	Permanent magnet speed n_2
1	300 rpm	5 µm	2 µm	20 rpm
2	500 rpm	3 µm	4 µm	40 rpm
3	700 rpm	1 µm	6 µm	60 rpm
4	900 rpm	0.5 µm	8 µm	80 rpm

Table 9. Experimental results when polishing with magnetic field SKD 61 coated Ni-P by Taguchi L16 method.

	Polishing mode					
No.	Workpiece speed (n_1)	AP diameter (A_P)	CIP diameter (C_P)	Magnet speed n_2	Roughness mean Ra_m (nm)	MRR (mg/min)
1	300 rpm	5 µm	2 µm	20 rpm	7,984	18,65
2	300 rpm	3 µm	4 µm	40 rpm	4,614	17,10
3	300 rpm	1 µm	6 µm	60 rpm	3,323	11,93
4	300 rpm	0.5 µm	8 µm	80 rpm	11,286	7,53
5	500 rpm	5 µm	4 µm	60 rpm	18,750	19,19
6	500 rpm	3 µm	2 µm	80 rpm	6,620	15,97
7	500 rpm	1 µm	8 µm	20 rpm	4,269	11,55
8	500 rpm	0.5 µm	6 µm	40 rpm	8,650	8,45
9	700 rpm	5 µm	6 µm	80 rpm	13,720	22,08
10	700 rpm	3 µm	8 µm	60 rpm	6,164	18,49
11	700 rpm	1 µm	2 µm	40 rpm	4,530	13,34
12	700 rpm	0.5 µm	4 µm	20 rpm	7,969	8,85
13	900 rpm	5 µm	6 µm	40 rpm	19,684	20,70
14	900 rpm	3 µm	8 µm	20 rpm	7,740	17,68
15	900 rpm	1 µm	4 µm	80 rpm	5,750	12,70
16	900 rpm	0.5 µm	2 µm	60 rpm	9,195	9,61

Polynomial equation with MRR and surface quality polishing with magnetic field SKD 61 coated Ni-P

Ra	$\mathrm{Ra} = 34.4951 = 0.306506 \times n_1 + 15.5759 \times A_P = 0.401054 \times C_P + 0.662524 \times n_2 + 0.000334337 \times {n_1}^2 + 0.00645375 \times n_1 \times A_P + 0.0022376 \times n_1 \times C_P = 0.000408744 \times n_1 \times n_2 = 1{,}56059 \times {A_P}^2 = 7.43918 \times A_P \times C_P + 0.504944 \times A_P \times n_2 + 0.668236 \times {C_P}^2 + 0.143539 \times C_P \times n_2 = 0.0219863 \times {n_2}^2$
MRR	$\mathrm{MRR} = \; = 49.3401 + 0.268705 \times n_1 = 4.96103 \times AP + 5.17166 \times C_P = 0.269363 \times n_2 = 0.0002474 \times {n_1}^2 = 0.0043546 \times n_1 \times A_P = 0.00555748 \times n_1 \times C_P + 0.000105134 \times n_1 \times n_2 + 1.0222 \times {A_P}^2 + 5.01039 \times A_P \times C_P = 0.361809 \times A_P \times N^2 = 0.679069 \times {C_P}^2 = 0.0970906 \times C_P \times n_2 + 0.0144638 \times {n_1}^2$

The results in Figure 6 show the ANOVA analysis of MRR highest with experimental parameters described in Table 9 for the S/N ratio corresponding to the workpiece speed, abrasive particle diameter, ferromagnetic particle size, and magnet speed are (-33.01), (-35.61), (-32.67) and (-22.64) levels for 4133 levels (corresponding workpiece speed $n_1 = 900$ rpm; AP diameter 5 µm; AP diameter 6 µm; Magnetic speed $n_2 = 60$ rpm).

The surface quality results obtained before and after polishing as described in Figure 8 show that the surface has been significantly improved by the proposed rotating magnetic field polishing method. With the experimental results obtained in Figure 7 and Table 9, when applying the proposed optimization algorithm OCMNO and ANOVA analysis to further improve the surface quality, the technological parameters are obtained when optimizing for the polishing process of materials SKD 61 coating Ni-P by rotating magnetic field as described in Table 10.

From the optimal results through ANOVA analysis and the proposed OCMNO algorithm, experimental verification processes are established. The verification experimental results depicted in Figure 8 after 60 min of polishing show that with the experimental analysis according to ANOVA for surface quality (Ra = 2.372 nm), the results show that the surface quality is improved better than the experimental according to Taguchi L16 as given in Table 5.

Factor	Average S/N by levels			
	Workpiece speed n_1	AP diameter	CIP diameter	Magnetic speed n_2
1	-12,70	-19,67	-13,35	-13,90
2	-16,19	-12,86	-14,88	-14,54
3	-14,36	-9,38	-14,38	-13,71
4	-16,44	-16,82	-16,13	-15,94
Mean	-14,92	-14,68	-14,68	-14,52
Max	-12,70	-9,38	-13,35	-13,71
Opt. plan	1313 (Workpiece speed n_1 300 rpm; AP diameter 1 µm; AP diameter 6 µm; Magnetic speed n_2 60 rpm)			

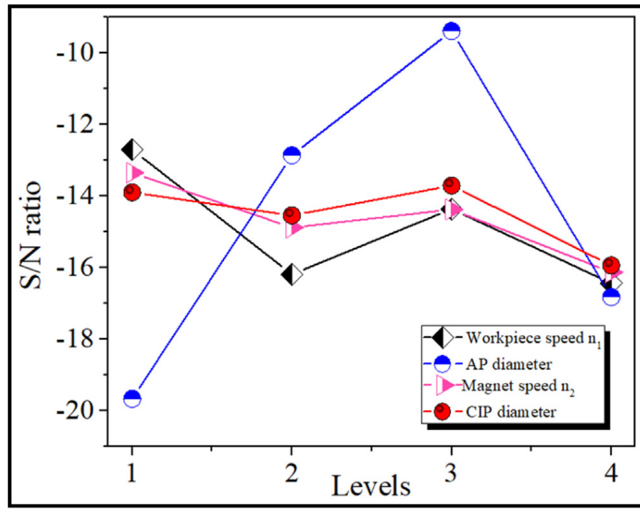

Fig. 5. Results of experimental analysis of ANOVA for polishing material SKD 61 coated Ni-P.

Factor	Average S/N by levels			
	Workpiece speed n_1	AP diameter	CIP diameter	Magnetic speed n_2
1	-31,83	-35,61	-32,52	-32,18
2	-31,67	-34,30	-32,38	-32,55
3	-32,54	-31,38	-32,67	-34,01
4	-33,01	-28,42	-32,15	-32,18
Min	-33,01	-35,61	-32,67	-22,64
Opt. plan	4133 (Workpiece speed 900 rpm; AP sizes 5 µm; CIP sizes 6 µm; Magnetic speed 60 rpm)			

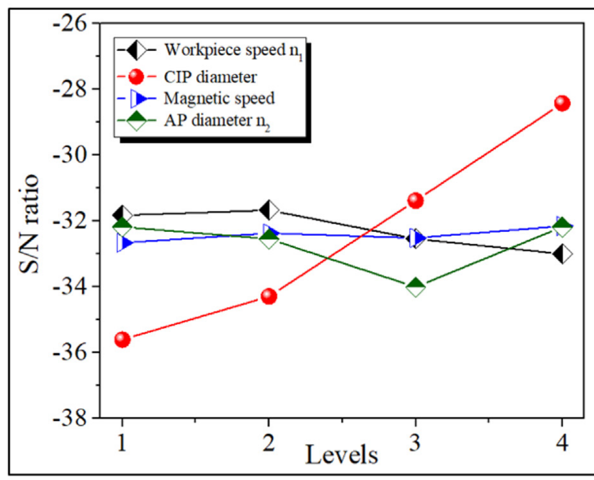

Fig. 6. Analysis of ANOVA for MRR polishing material SKD 61 coated Ni-P.

However, the surface under optimal conditions with experimental analysis of ANOVA still appears a few very small scratches. The ultra-smooth surface with no scratches on the surface obtained experimentally according to the polishing parameters proposed by the OCMNO optimization algorithm. Experimenting according to the technological mode proposed by OCMNO gives the superfine surface quality with Ra = 1.137 nm, along with that, the surface quality is improved by 52.08% compared to the optimization according to the experimental analysis ANOVA. Experimental according to the polishing technology parameters proposed by OCMNO and ANOVA for the material removed rate 29.78 and 23.05 mg/min, through which the ability to material removed rate increased to 29.19% compared to the optimal according to experimental analysis ANOVA. The obtained results show that the optimization algorithm and the proposed polishing model are capable of creating an ultra-smooth surface for SKD 61 coated Ni-P material without any scratches.

4 Conclusions

In this work, a new OCMNO optimization algorithm is proposed. On the basis of the presented optimization model based on the flexibility and strong convergence of the OCMNO algorithm, the technological parameters in the polishing of SKD 61 coated Ni-P materials by using MCF in the rotating magnetic field produced by the proposed OCMNO algorithm to create surface quality in nanometer form. The main results of the study are as described below:

– A new OCMNO algorithm is proposed based on NLO. The analytical procedures include benchmark functions to evaluate the performance of the presented optimization algorithms in terms of solution, quality and speed of convergence. The analysis results show that the quality obtained by the proposed OCMNO algorithm is superior to the mentioned algorithms in most cases. Therefore, the proposed OCMNO algorithm exhibits high applicability for nonlinear systems and other optimization problems.

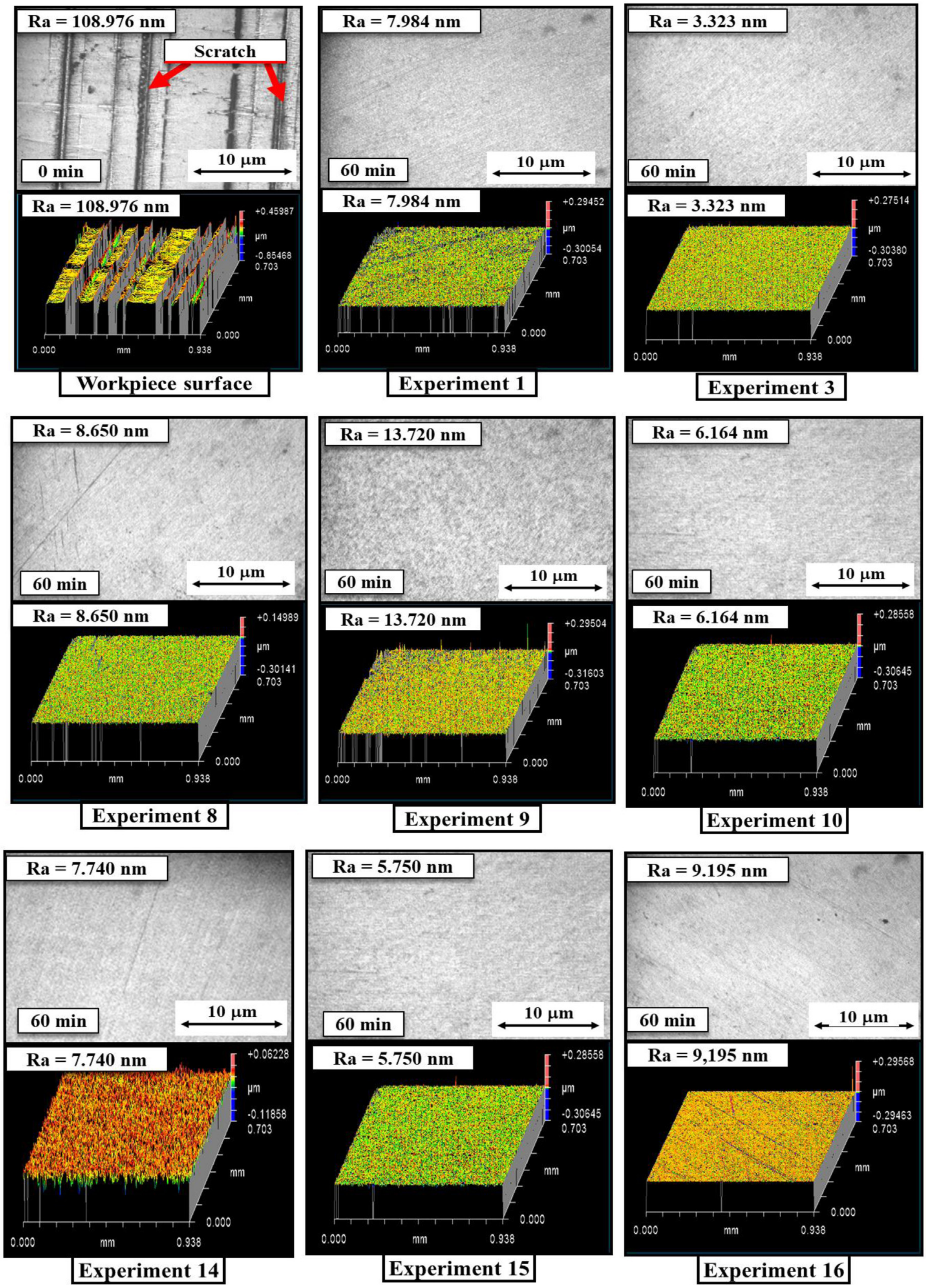

Fig. 7. Morphology of some workpiece surface SKD 61 coated Ni-P before and after polishing.

Table 10. Optimal polishing parameters according to ANOVA and OCMNO analysis.

Optimize polishing mode	Workpiece speed n_1	AP diameter	CIP diameter	Magnet speed n_2
Ra optimize by ANOVA	300 rpm	1 μm	6 μm	60 rpm
Ra optimize by OCMNO	318.65 rpm	1.5 μm	4.5 μm	52.17 rpm
MRR optimize by ANOVA	900 rpm	5 μm	6 μm	60 rpm
MRR optimize by OCMNO	832.67 rpm	4.5 μm	7.5 μm	58.33 rpm

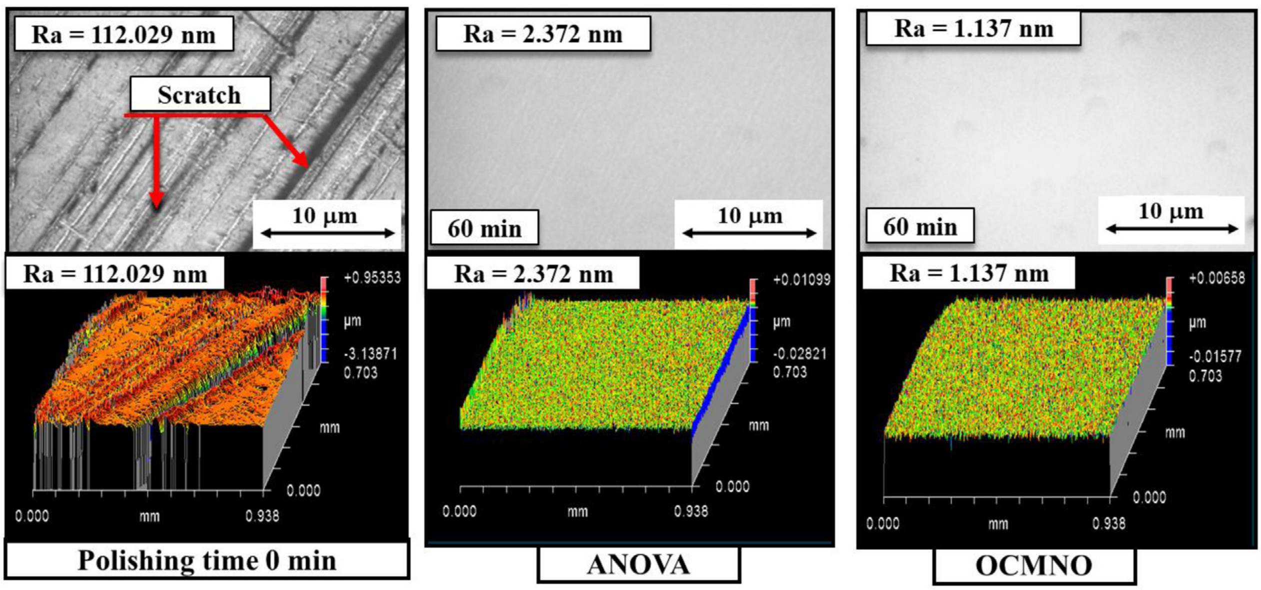

Fig. 8. Surface morphology when machining verified under optimal cutting modes.

– Experimental results of polishing with rotating magnetic field for SKD 61 coated Ni-P material capable of creating ultra-smooth surface with surface roughness obtained in nanometer form when following the technological parameters by the algorithm OCMNO suggested. The verification experiments obtained superfine surface with Ra = 1.137 nm according the workpiece speed n_1, AP diameter, CIP diameter, and magnet speed n_2 with polishing parameters 318.65 rpm, 1.5 μm, 4.5 μm and 52.17 rpm, respectively. The optimized surface quality has been increased by 52.08 % when choosing technological parameters according to the OCMNO optimization algorithm compared to the results of the experimental optimization analysis. Besides that the material removed rate can increased to 29.19% compared to the optimal according to experimental analysis ANOVA. The proposed polishing and optimization model is capable of obtaining superfine surface in nanometer form for SKD 61 coated Ni-P material from inexpensive polishing materials such as commercial CIP, AP particles. Thereby creating great potential in ultra-precision machining of SKD 61 coated Ni-P materials in particular as well as materials in mold processing in general.

Nomenclature

OCMNO	Optimization collaborative of multiple nonlinear systems
MCF	Magnetic Compound Fluid
AI	Artificial intelligence
NLO	Nonlinear objects
DTP	Displays the optimal target parameter
N_V	Decision variables
V_{MAX}	Largest limit of decision variables
V_{MIN}	Smallest limit of decision variables
η	Average parameter
δ	Standard deviation
k	Random number in the range [0,1]
E_T	Time taken by the search task of OCMNO
ME	Motion factor
WD	Index refers to the dependent NLO with the lowest DTP
S.CA	Stop criterion of the algorithm
TLBO	Teaching–learning-based optimization
GSA	Gravitational Search Algorithm
PSO	Particle Swarm Optimization
ABC	Artificial Bee Colony

AP	Abrasive particles
CIP	Carbonyl iron particles
ANOVA	Analysis of Variance
S/N ratio	Signal-to-noise ratio
$P_{\mathrm{NLO}[M]}$	Location of the main NLO

References

1. A.A. Ramírez-Duque, A. Frizera-Neto, T.F. Bastos, Robot-assisted autism spectrum disorder diagnostic based on artificial reasoning, J. Intell. Robotic Syst. **96** (2019) 267–281
2. F. Al-Mufti, V. Dodson, J. Lee, E. Wajswol, C. Gandhi, C. Scurlock, C. Cole, K. Lee, S.A. Mayer, Artificial intelligence in neurocritical care, J. Neurolog. Sci. **404** (2019) 1–4
3. K. Jha, A. Doshi, P. Patel, M. Shah, A comprehensive review on automation in agriculture using artificial intelligence, Artific. Intell. Agric. **2** (2019) 1–12
4. M. Soori, B. Arezoo, R. Dastres, Machine learning and artificial intelligence in CNC machine tools, a review, Sustain. Manufactur. Serv. Econ. **57** (2023) 708–726
5. G. Shankarrao Patange, A. Bharatkumar Pandya, How artificial intelligence and machine learning assist in industry 4.0 for mechanical engineers, Mater. Today: Proc. **72** (2023) 622–625
6. X.-S. Yang, A new metaheuristic bat-inspired algorithm, in *Nature Inspired Cooperative Strategies for Optimization (NICSO 2010)*, edited by J.R. González, D.A. Pelta, C. Cruz, G. Terrazas, N. Krasnogor (Springer Berlin Heidelberg, Berlin, Heidelberg, 2010), pp. 65–74
7. D. Hoang Tien, T. Duc Quy, T. Pham Thi Thieu, N.D. Trinh, Application of vibration singularity analysis, stochastic tool wear, and GPR-MOPSO hybrid algorithm to monitor and optimise power consumption in high-speed milling, Manufactur. Rev. **9** (2022) 14–27
8. R.R. Chakule, S.S. Chaudhari, K.V. Chandratre, P.B. Patole, P.S. Talmale, Nanofluids, micro-lubrications and machining process optimisations – a review, Manufactur. Rev. **10** (2023) 1–20
9. A. Amirteimoori, I. Mahdavi, M. Solimanpur, S.S. Ali, E.B. Tirkolaee, A parallel hybrid PSO-GA algorithm for the flexible flow-shop scheduling with transportation, Comput. Ind. Eng. **173** (2022) 108672
10. Q. Yu, T. Zhou, Y. He, P. Liu, X. Wang, Y. Jiang, J. Yan, Annealed high-phosphorus electroless Ni–P coatings for producing molds for precision glass molding, Mater. Chem. Phys. **262** (2021) 124297
11. D. Nguyen, J. Wu, N.M. Quang, L.A. Duc, P.X. Son, Applying fuzzy grey relationship analysis and Taguchi method in polishing surfaces of magnetic materials by using magnetorheological fluid, Int. J. Adv. Manufactur. Technol. **112** (2021) 1675–1689
12. R. Kang, Y. Zhang, S. Gao, J. Huang, X. Zhu, High surface integrity fabrication of silicon wafers using a newly developed nonwoven structured grind-polishing wheel, J. Manufactur. Process. **77** (2022) 229–239
13. W.-L. Zhu, A. Beaucamp, Compliant grinding and polishing: a review, Int. J. Mach. Tools Manufact. **158** (2020) 103634
14. L.A. Duc, P.M. Hieu, N.M. Quang, Study chemical reaction of –Si–OH surface layer by solid and ionic form to surface quality when polishing with chemical–mechanical slurry, J. King Saud Univ. Eng. Sci. **35** (2022) 1–9
15. J. Bai, Z. Xu, L. Qian, Precision-improving manufacturing produces ordered ultra-fine grained surface layer of tungsten heavy alloy through ultrasonic elliptical vibration cutting, Mater. Des. **220** (2022) 110859
16. A. Lu, Z. Shang, X. Luo, T. Jin, H. Luo, Rapid fabrication of ultra-smooth Y-TZP bioceramic surfaces by dual-axis wheel polishing: process development and tribological characterization, J. Manufactur. Process. **55** (2020) 276–287
17. T. Hirata, Y. Takei, H. Mimura, Machining property in smoothing of steeply curved surfaces by elastic emission machining, Proc. CIRP **13** (2014) 198–202
18. M. Kanaoka, H. Takino, K. Nomura, Y. Mori, H. Mimura, K. Yamauchi, Removal properties of low-thermal-expansion materials with rotating-sphere elastic emission machining, Sci. Technol. Adv. Mater. **8** (2007) 170–172
19. N.T. Duy, D.H. Tien, P.T.T. Thoa, A new environment-friendly magnetorheological finishing and fuzzy grey relation analysis in Ti-6Al-4V alloy polishing, Manufactur. Rev. **9** (2022) 17
20. C. Xiao, F.-C. Hsia, A. Sutton-Cook, B. Weber, S. Franklin, Polishing of polycrystalline diamond using synergies between chemical and mechanical inputs: a review of mechanisms and processes, Carbon **196** (2022) 29–48
21. C. Wang, Y.M. Loh, C.F. Cheung, S. Wang, L.T. Ho, Z. Li, Shape-adaptive magnetic field-assisted batch polishing of three-dimensional surfaces, Precis. Eng. **76** (2022) 261–283
22. Z. Xia, F. Fang, E. Ahearne, M. Tao, Advances in polishing of optical freeform surfaces: a review, J. Mater. Process. Technol. **286** (2020) 116828
23. D.H. Tien, T.N. Duy, P.T.T. Thoa, Applying GPR-FGRA hybrid algorithm for prediction and optimization of eco-friendly magnetorheological finishing Ti–6Al–4V alloy, Int. J. Interactive Des. Manufactur. **17** (2022) 729–745
24. D. Zhou, X. Huang, Y. Ming, X. Li, H. Li, W. Li, Material removal characteristics of magnetic-field enhanced shear thickening polishing technology, J. Mater. Res. Technol. **15** (2021) 2697–2710
25. J.O. Obiko, F.M. Mwema, M.O. Bodunrin, Validation and optimization of cutting parameters for Ti-6Al-4V turning operation using DEFORM 3D simulations and Taguchi method, Manufactur. Rev. **8** (2021) 5–13
26. S. Kumar, G.H.V.C. Chary, M.G. Dastidar, Optimization studies on coal–oil agglomeration using Taguchi (L16) experimental design, Fuel **141** (2015) 9–16
27. A. Jain, B.J. Bora, R. Kumar, P. Sharma, B. Deepanraj, K. Irshad, C. Ravikiran, Application of hybrid Taguchi L16 and desirability for model prediction and optimization in assessment of the performance of a novel Water Hyacinth biodiesel run diesel engine, Fuel **339** (2023) 127377
28. B. Karmakar, B. Ghosh, S. Samanta, G. Halder, Sulfonated catalytic esterification of Madhuca indica oil using waste Delonix regia: L16 Taguchi optimization and kinetics, Sustain. Energy Technolog. Assess. **37** (2020) 100568

Cite this article as: Le Anh Duc, Pham Minh Hieu, Nguyen Minh Quang, Development of OCMNO algorithm applied to optimize surface quality when ultra-precise machining of SKD 61 coated Ni-P materials, Manufacturing Rev. **10**, 7 (2023)